Contrasting phagosome pH regulation and maturation in human M1 and M2 macrophages

Johnathan Canton[a], Rojyar Khezri[a], Michael Glogauer[b], and Sergio Grinstein[a,c]
[a]Program in Cell Biology, Hospital for Sick Children, Toronto, ON M5G 0A4, Canada; [b]Faculty of Dentistry, University of Toronto, Toronto, ON M5G 1G6, Canada; [c]Keenan Research Centre of the Li Ka Shing Knowledge Institute, St. Michael's Hospital, Toronto, ON M5C 1N8, Canada

ABSTRACT Macrophages respond to changes in environmental stimuli by assuming distinct functional phenotypes, a phenomenon referred to as macrophage polarization. We generated classically (M1) and alternatively (M2) polarized macrophages—two extremes of the polarization spectrum—to compare the properties of their phagosomes. Specifically, we analyzed the regulation of the luminal pH after particle engulfment. The phagosomes of M1 macrophages had a similar buffering power and proton (equivalent) leakage permeability but significantly reduced proton-pumping activity compared with M2 phagosomes. As a result, only the latter underwent a rapid and profound acidification. By contrast, M1 phagosomes displayed alkaline pH oscillations, which were caused by proton consumption upon dismutation of superoxide, followed by activation of a voltage- and Zn^{2+}-sensitive permeation pathway, likely H_V1 channels. The paucity of V-ATPases in M1 phagosomes was associated with, and likely caused by, delayed fusion with late endosomes and lysosomes. The delayed kinetics of maturation was, in turn, promoted by the failure of M1 phagosomes to acidify. Thus, in M1 cells, elimination of pathogens through deployment of the microbicidal NADPH oxidase is given priority at the expense of delayed acidification. By contrast, M2 phagosomes proceed to acidify immediately in order to clear apoptotic bodies rapidly and effectively.

INTRODUCTION

Macrophages carry out a broad variety of functions, ranging from clearance of invading pathogens to the resolution of inflammation and the maintenance of homeostasis during tissue repair and development. The functional versatility of macrophages is in part due to their phenotypic plasticity. Macrophages respond to environmental stimuli by assuming distinct, metastable functional phenotypes—a phenomenon referred to as macrophage polarization. The complex-

Abbreviations used: CcA, concanamycin A; CCCP, carbonyl cyanide *m*-chlorophenyl hydrazone; DPI, diphenyleneiodonium; FITC, fluorescein isothiocyanate; GM-CSF, granulocyte macrophage colony-stimulating factor; H_V1, voltage-gated proton channel; LAMP-1, lysosome-associated membrane protein 1; M-CSF, macrophage colony-stimulating factor; NBT, nitroblue tetrazolium; NOX, NADPH oxidase; PLY, pneumolysin; ROS, reactive oxygen species; SOZ, serum-opsonized zymosan; TfR, transferrin receptor; V-ATPase, vacuolar ATPase.

ity and varying nature of such stimuli cause the cells to polarize into a continuum of phenotypes or "shades" (Mosser and Edwards, 2008) that are difficult to segregate and hence to study in isolation. A convenient, albeit imperfect alternative to studying macrophage polarization has been to analyze the extremes of the spectrum: classically activated macrophages (M1) and alternatively activated macrophages (M2). The M1 phenotype is generally induced by proinflammatory cues such as bacterial infection, Toll-like receptor ligation, and exposure to the T-helper 1 cytokine interferon-γ (IFN-γ) and is characterized by an increased capacity to clear microbes and tumors, as well as by enhanced antigen-presenting efficiency (Lawrence and Natoli, 2011). In contrast, the M2 phenotype is induced through stimulation by the STAT-6–activating cytokines interleukin-4 (IL-4) and/or IL-13 and serves homeostatic functions such as clearance of apoptotic cells and debris, tissue repair and remodeling, and suppression of inflammation (Galli *et al.*, 2011).

The process of phagocytosis is essential to both M1- and M2-specific functions. Indeed, a hallmark of M1 macrophages is their potent microbicidal capacity, which entails the engulfment and delivery of pathogens to a degradative phagolysosome. Phagocytosis is also key for the processing and delivery of exogenous antigens to

the MHC-II compartment (Blum *et al.*, 2013) for eventual presentation at the cell surface (Hufford *et al.*, 2011; Uderhardt *et al.*, 2012; Short *et al.*, 2013). Instruction of the adaptive arm of the immune response by antigen presentation is a characteristic feature of M1 macrophages (Lawrence and Natoli, 2011). In contrast, and in line with their homeostatic function, M2 macrophages use phagocytosis for the clearance of products of tissue wear and tear, such as apoptotic and necrotic cells. Proper recognition of phagocytic targets by the intended subset of macrophages is critical: aberrant sorting of apoptotic cells to M1 macrophages results in the presentation of self-antigen and the development of autoimmune disease (Uderhardt *et al.*, 2012). The deleterious consequences of aberrant phagocytosis suggest that the processes downstream of target binding and uptake, collectively known as phagosome maturation, must be significantly different in M1 versus M2 macrophages. Whether and how phagosome maturation differs between polarized macrophages, however, remains unclear.

In macrophages, phagosome maturation is associated with progressive luminal acidification, which is attributed to the gradual accretion of active vacuolar ATPases (V-ATPases) upon fusion with compartments of the endolysosomal pathway. The rate and extent of the acidification, however, are influenced by a variety of other factors, which include the permeability of the phagosomal membrane to counterions, the luminal buffering power, and the rate of proton (equivalent) leakage. Proton consumption by chemical reactions can also affect the course of acidification. The prevailing phagosomal pH dictates the efficiency of microbial killing and antigen presentation, as well as the degradation of effete cells and the resorption of their components for recycling. Of importance, the pH optimum of these processes is not the same. It is therefore conceivable that the rate and/or extent of phagosome acidification may be different in M1 and M2 macrophages, possibly accounting for the negative consequences of aberrant target sorting. To date, however, the kinetics and determinants of phagosomal acidification have not been compared in M1 and M2 cells.

In this study, ratio imaging was used to monitor the luminal pH of phagosomes formed by M1 and M2 macrophages derived from human blood monocytes. Striking differences were noted, and the underlying mechanisms were studied in detail. In addition, the functional consequences of luminal acidification were investigated and are discussed in the context of the specialized role of polarized macrophages.

RESULTS
Phagosomal pH differs markedly in M1 versus M2 macrophages
M1 macrophages were generated by exposing human monocytes to granulocyte macrophage colony-stimulating factor (GM-CSF) for 5 d, followed by stimulation with IFN-γ and lipopolysaccharide (LPS) for an additional 2 d. To generate M2 macrophages, monocytes were stimulated with macrophage colony-stimulating factor (M-CSF) for 5 d, followed by IL-4 for 2 d. We confirmed the occurrence of polarization measuring CD80 and CD200r (Supplemental Figure S1A), recently identified reliable markers for M1 and M2 cells, respectively (Jaguin *et al.*, 2013). Moreover, the macrophages displayed either "fried-egg" or elongated morphology (Supplemental Figure S1B), consistent with M1 and M2 polarization, respectively (McWhorter *et al.*, 2013). We verified that the macrophage populations were not contaminated by monocyte-derived dendritic cells; the M1 and M2 cells were devoid of the dendritic cell–specific marker CD1a, which, in contrast, was abundant in dendritic cells (Supplemental Figure S1A) derived from the same population of

monocytes by culturing them in GM-CSF and IL-4 for 7 d (Zizzo *et al.*, 2012).

M1 and M2 macrophages exhibit differential expression of phagocytic receptors (Mantovani *et al.*, 2004). To analyze phagosome acidification in M1 and M2 macrophages under comparable conditions, we sought and identified a phagocytic target that was taken up efficiently by both phenotypes, namely serum-opsonized zymosan (SOZ). Before opsonization, zymosan particles were labeled with a pH-sensitive fluorophore of $pK_a \approx 6.3$, suitable for measurements of phagosomal pH (Steinberg and Grinstein, 2007). A high-resolution system that combines fluorescence ratio imaging with continuous bright-field microscopy was used to identify macrophages that bound labeled SOZ and to measure the pH of the resulting phagosomes as described in *Materials and Methods*. Using this method, we observed striking differences in the behavior of M1 and M2 cells. Phagosomes formed by M1 macrophages remained near neutrality for at least 30 min after formation, with an average pH of 7.55 ± 0.16. In contrast, M2 phagosomes acidified rapidly, reaching a steady-state pH of 4.99 ± 0.18 within 10 min (Figure 1, A and C). The acidification recorded in M2 phagosomes was prevented by concanamycin A (CcA), confirming the involvement of V-ATPases (Figure 1, B and C). We next explored the mechanisms underlying the differential regulation of pH in these macrophage phenotypes.

M1 macrophages produce more intraphagosomal reactive oxygen species than M2 macrophages
Proton consumption by biochemical reactions is an important determinant of phagosomal pH in neutrophils (Segal *et al.*, 1981; Jankowski *et al.*, 2002) and dendritic cells (Savina *et al.*, 2006; Mantegazza *et al.*, 2008), where superoxide generated by the NADPH oxidase (NOX2) can undergo dismutation to hydrogen peroxide. We considered whether a similar mechanism was responsible for the limited acidification of M1 phagosomes, in light of the increased expression of the oxidase reportedly induced by M1-polarizing factors like IFN-γ and LPS (Cassatella *et al.*, 1990; Amezaga *et al.*, 1992; Casbon *et al.*, 2012). Superoxide generation was initially assessed in individual M1 or M2 phagosomes using nitroblue tetrazolium (NBT). While OxyBurst has been the method of choice to monitor reactive oxygen species (ROS) in phagosomes, we found NBT to be a superior reagent for the following reasons: 1) unlike OxyBurst fluorescence, which is sensitive to the surrounding pH, we found the deposition of formazan from NBT to be independent of pH (Supplemental Figure 2, A and B); 2) unreacted OxyBurst can be activated by the excitation light of the fluorescence microscope (Supplemental Figure 2C), whereas the light required to visualize formazan is without effect (Supplemental Figure 2D); 3) activated OxyBurst is susceptible to photobleaching by the excitation light (Supplemental Figure 2E); and 4) because it is attached covalently to zymosan, the amount of OxyBurst available to monitor ROS formation is finite. By contrast, the membrane permeant NBT can enter the phagosome in unlimited amount (Supplemental Figure 2F).

The rate and extent of deposition of formazan were considerably greater in M1 than in M2 phagosomes (Figure 2A). In fact, while formazan deposits were readily observed in M1 phagosomes when using 1 µg/ml NBT, they were only visible in a fraction of M2 phagosomes even when using a 10-fold higher concentration (10 µg/ml) of NBT (Figure 2A). The large difference in reactive oxygen species (ROS) generation was verified using luminol, adding superoxide dismutase and catalase 10 min after phagocytosis was initiated to selectively analyze intracellular (largely intraphagosomal) ROS generation (Dahlgren *et al.*, 2007). As illustrated in Figure 2, B and C,
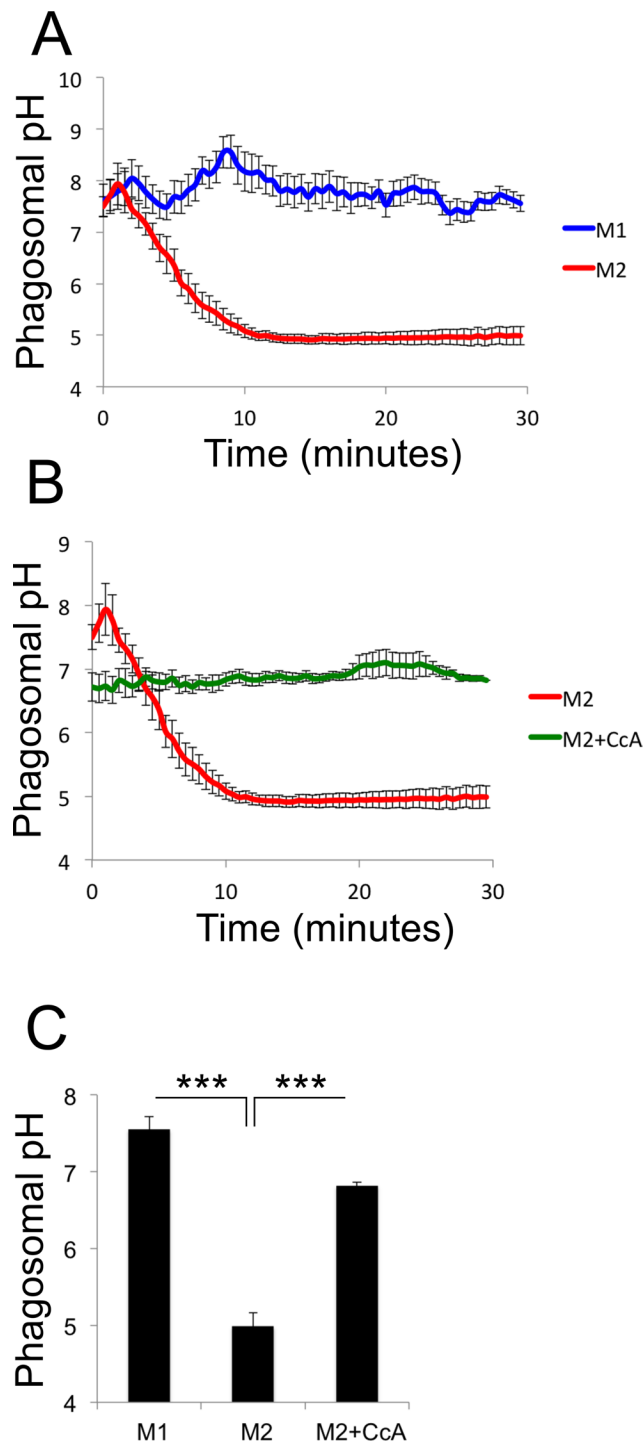
FIGURE 1: Phagosomes acidify in M2 macrophages but maintain near-neutral pH in M1 macrophages. (A) Macrophages were challenged with serum-opsonized fluorescein isothiocyanate-conjugated zymosan (FITC-SOZ), and upon particle binding, pH measurements were made every 30 s for 30 min by ratiometric fluorescence imaging, as detailed in *Materials and Methods*. M1 macrophages are shown in blue and M2 macrophages in red. (B) M2 macrophages were treated with 2 µM concanamycin A (CcA, green) or left untreated (red, replicated from A), and phagosomal pH measurements were performed as in A. (C) The graph compares phagosomal pH values obtained as in A, 30 min after completion of phagocytosis. Data represent the means ± SEM of 6–13 independent experiments using cells from at least three separate donors. ***$p \leq 0.001$.

ROS production was much greater and more sustained in M1 than in M2 phagosomes, in good agreement with the formazan deposition determinations.

The greater capacity of M1 cells to generate ROS is at least partly due to their higher expression of NOX2. Quantitative immunoblotting revealed that the transmembrane components of the NADPH oxidase—the gp91 and p22 subunits—are more abundant in M1 than in M2 cells (Figure 2D-E).

M1 phagosomes retain NOX2, which is rapidly lost from M2 phagosomes

The net generation of ROS is much greater in M1 than in M2 macrophages not only because of their higher NOX2 content, but also because the oxidase remains active longer. This became apparent when monitoring the rate of superoxide generation over time in single phagosomes, incubating the cells in the presence of subsaturating concentrations of NBT (1 µg/ml for M1 and 10 µg/ml for M2 macrophages). Using bright-field microscopy, we could estimate the rate of formazan deposition by acquiring images at regular intervals and quantifying the progressive decrease in pixel intensity. As illustrated in Figure 3A and summarized in Figure 3, B and C, whereas M1 phagosomes generate ROS continuously for at least 30 min, the oxidase activity of M2 phagosomes becomes undetectable after 5–10 min.

The rapid termination of oxidase activity in M2 phagosomes was associated with, and likely caused by, the removal of the transmembrane subunits from the phagosome. This became apparent after fixation and immunostaining of samples at defined intervals after phagocytosis was completed (Figure 3, D and E). By measuring the fluorescence signal of individual phagosomes, we quantified the extent of removal of the gp91 or p22 subunits of the oxidase from the phagosomal membrane (Figure 3F and Supplemental Figure S3B). In addition, using the scoring system illustrated in Supplemental Figure S3A, we determined the relative distribution of gp91- or p22-positive phagosomes at the indicated times (Figure 3, G and H, and Supplemental Figure S3, C and D). Regardless of the method used for quantitation, it is clear that the oxidase persists in the membrane of M1 phagosomes for extended periods (Figure 3, D, F, and G, and Supplemental Figure S3, B and C), whereas it is rapidly removed from M2 phagosomes (Figure 3, E, F, and H, and Supplemental Figure S3, B and D), accounting at least in part for their rapid termination of intracellular ROS production.

Phagosome-lysosome fusion is delayed in M1 macrophages

After sealing, the phagosomal membrane undergoes extensive remodeling, a result of multiple fusion and fission events with other endomembrane compartments. The differential rate of clearance of the NADPH oxidase from M1 and M2 phagosomes suggests that maturation proceeds at different rates and/or by different routes in the two types of macrophages. To determine whether this was indeed the case, we measured the course of acquisition and loss of several endomembrane markers from M1 or M2 phagosomes. Macrophages were challenged with labeled SOZ, and after 5 min of phagocytosis, external or incompletely internalized particles were identified by addition of fluorescently labeled antibodies. By subsequently omitting from consideration the antibody-tagged particles, we were able to more precisely demarcate the initiation of the maturation period in the untagged (fully internalized) SOZ. As illustrated in Figure 4, A and B, transferrin receptors (TfRs), which are indicative of early/recycling endosomes, were acquired very rapidly by M2 phagosomes and disappeared shortly thereafter, as lysosome-associated membrane protein 1 (LAMP-1) was recruited. The later stages of acquisition of
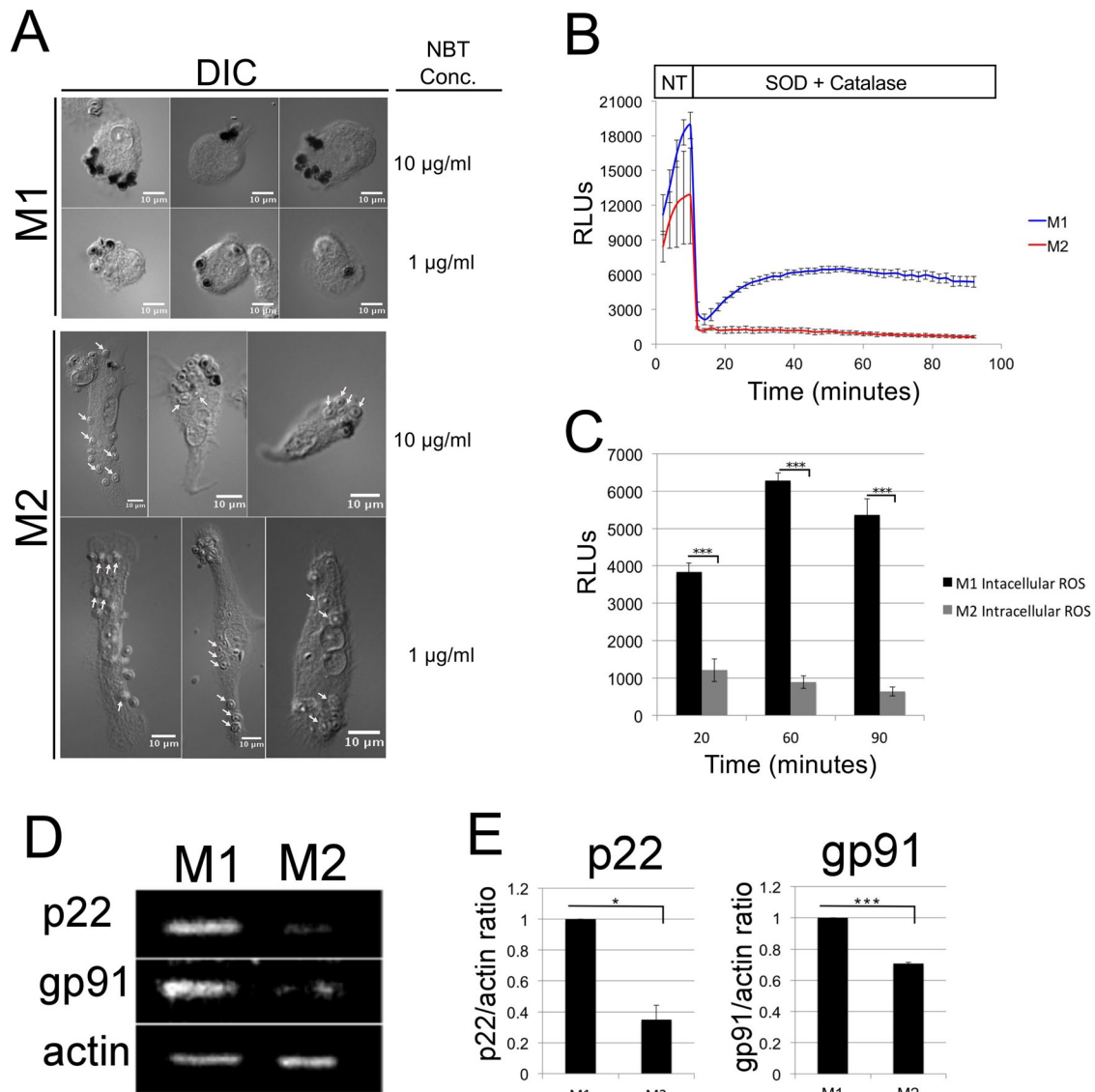
FIGURE 2: M1 macrophages produce more intraphagosomal reactive oxygen species than M2 macrophages. (A) Macrophages were challenged with SOZ for 30 min in the presence of NBT at 1 or 10 µg/ml, as indicated. Cells were then washed three times with PBS, fixed with 2% paraformaldehyde, and imaged by differential interference contrast microscopy. Dark formazan deposits indicate local production of superoxide. White arrows indicate SOZ-containing phagosomes that are negative for formazan deposits. Scale bars, 10 µm. (B, C) Macrophages were challenged with SOZ in the presence of 8 U/ml HRP. After 1 min of phagocytosis, excess SOZ was washed off and the cells bathed in PBS containing 10 mM glucose, 8 U/ml HRP, and 50 µM luminol. Luminescence was measured for 10 min (no treatment [NT]), and then superoxide dismutase (SOD; 50 U/ml) and catalase (2000 U/ml) were added to eliminate extracellular ROS. Luminescence was measured for an additional 80 min. (C) Luminescence determinations 20, 60, and 90 min after the addition of SOD and catalase. Data are displayed as relative luminescence units (RLUs) over time and represent the mean ± SEM from three independent experiments using cells from two donors. (D) Differentiated M1 and M2 macrophages were lysed and separated by 12% SDS–PAGE. Images show immunoblots for p22, gp91, and actin. (E) Quantitation of multiple experiments like that in D. The p22/actin and gp91/actin ratios are depicted. Data represent the mean ± SEM from three independent experiments using cells from two donors. *$p < 0.05$, ***$p \leq 0.001$.

LAMP-1, a late endosome-lysosome marker, corresponded to the time of acquisition of labeled dextran, which was chased after pulsing (see *Materials and Methods*) to serve as a lysosomal marker. This pattern of rapid maturation is somewhat faster than that described for unpolarized primary and immortalized macrophages (Tsang *et al.*, 2000; Sokolovska *et al.*, 2013) and is compatible with the rapid acquisition of V-ATPases deduced from pH measurements. In stark contrast, M1 phagosomes retained TfR longer and acquired LAMP-1 and dextran more slowly and less completely than their M2 counterparts. The delayed maturation of M1 phagosomes is consistent with the prolonged residence of gp91 and p22 on their membrane and the sustained phagosomal oxidase activity.

Inhibition of the NADPH oxidase enables acidification of phagosomes in M1 macrophages

We next explored whether the increased NADPH oxidase activity of M1 macrophages was responsible for the maintenance of
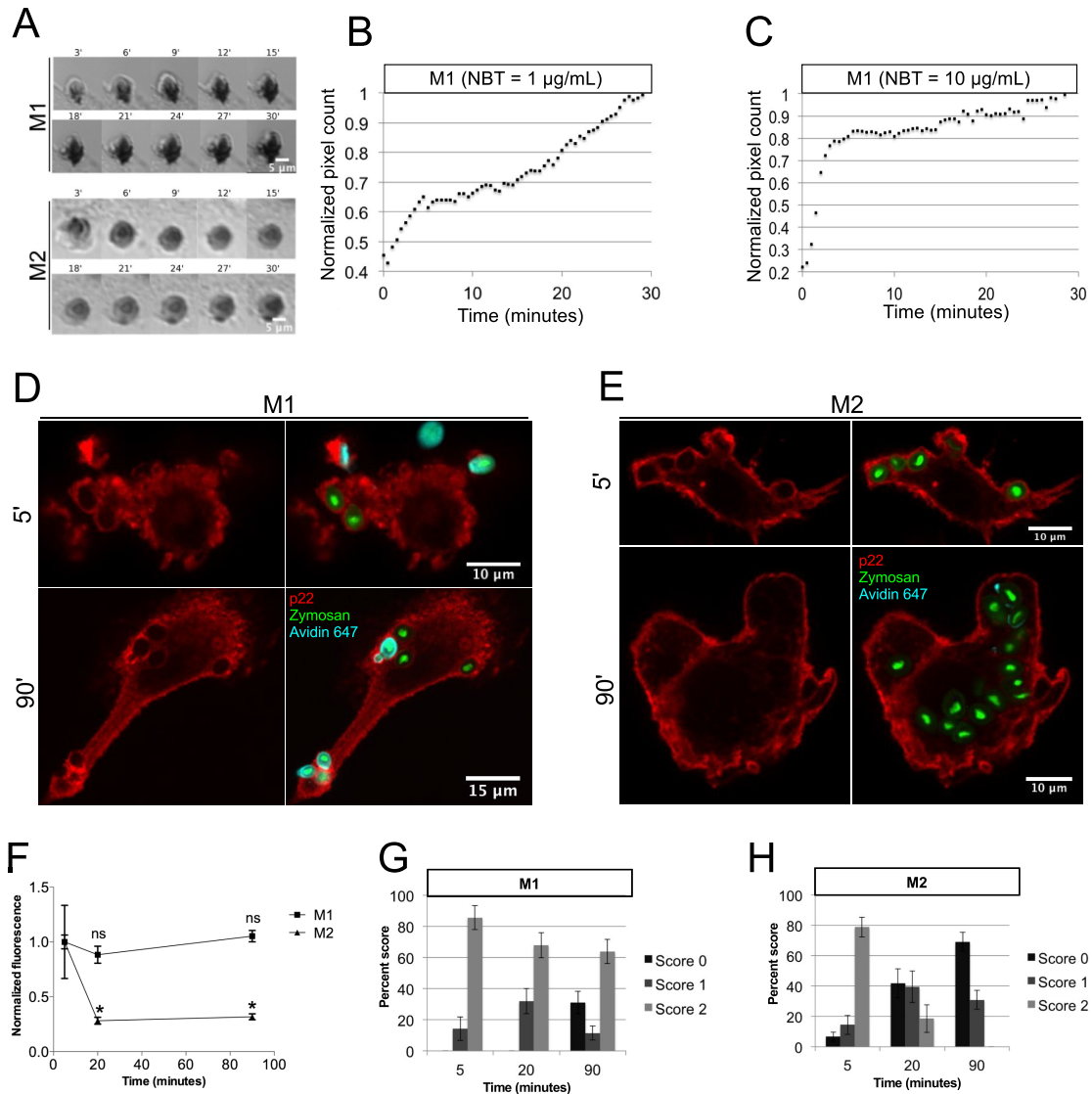
FIGURE 3: The NADPH oxidase is retained on M1 phagosomes but rapidly lost from M2 phagosomes. (A–C) Macrophages were challenged with SOZ for 1 min in the presence of NBT at 1 or 10 µg/ml. Excess SOZ was washed off with PBS, followed by incubation at 37°C in HEPES-buffered RPMI with 1 or 10 µg/ml NBT, acquiring pictures every 30 s for 30 min. (A) Images of individual phagosomes acquired at the indicated times during maturation for M1 (top) and M2 (bottom) macrophages. Scale bar, 5 µm. (B, C) Deposition of formazan was quantified using ImageJ and is depicted relative to the maximum value for each phagosome. Measurements for M1 macrophages were performed using 1 µg/ml NBT, as 10 µg/ml resulted in early signal saturation; for M2 macrophages, measurements were performed using 10 µg/ml NBT, as no signal could be detected at 1 µg/ml due to the low level of ROS production in these cells. Data represent deposition of formazan in a single phagosome, representative of three independent experiments. (D–H) Macrophages were challenged with biotinylated, FITC-labeled SOZ sedimented onto the cells by centrifugation for 1 min. Cells were incubated for 4 min at 37°C, then immediately placed on ice-cold PBS with streptavidin 647 to label incompletely internalized particles. The cells were then washed with ice-cold PBS, and the 5-min time-point coverslips were fixed with ice-cold methanol. The 20- and 90-min time-point coverslips were incubated for an additional 15 and 85 min, respectively, at 37°C and then fixed with ice-cold methanol. All coverslips were immunostained with a p22 monoclonal antibody and imaged by confocal microscopy. (D, E) Representative confocal images. (F) The fluorescence signal derived from the p22 monoclonal antibody at the phagosome membrane was quantified in images like those in D and E. Data in F represent the normalized mean fluorescence ± SEM from 30 phagosomes from three experiments. (G, H) Percentage of phagosomes with score 2, 1, or 0 (see Supplemental Figure S3 for scoring criteria) for p22 at the indicated time points in M1 (G) or M2 (H) macrophages. Data are means ± SEM from three independent experiments using cells from different donors.

near-neutral pH in their phagosomes (Figure 1A). Treatment with diphenyleneiodonium (DPI), a potent oxidase inhibitor, unmasked an acidification of phagosomes (Figure 5A). However, despite the absence of oxidase activity, the phagosomes in M1 macrophages acidified more slowly than those in M2 cells (Figure 5A). Thus factors other than the rate of proton consumption by dismutation of superoxide must contribute to the differential behavior of M1 and M2 phagosomes.
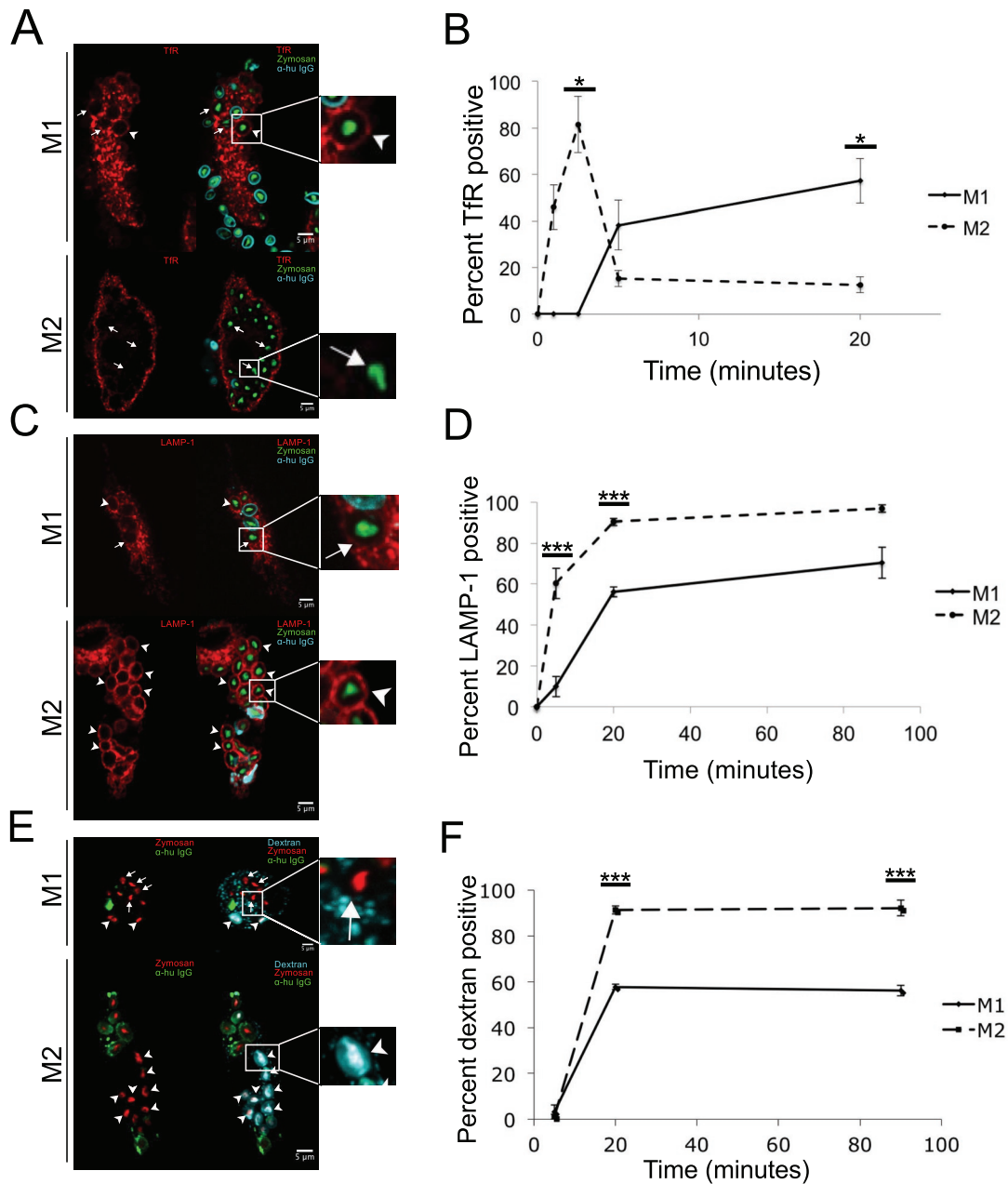
FIGURE 4: M1 macrophages exhibit delayed phagosome-lysosome fusion kinetics. Macrophages were challenged with either FITC-labeled SOZ or tetramethyl rhodamine–labeled SOZ and centrifuged for 1 min, and unbound particles were washed with PBS. Cells were incubated for 4 min at 37°C, then immediately placed on ice-cold PBS with anti-human IgG 647 (A–D) or anti-human IgG 488 (E, F) to label incompletely internalized zymosan particles. Cells were then incubated at 37°C in RPMI for the indicated times, fixed with either ice-cold methanol (A–D) or 2% paraformaldehyde (E, F), and immunostained for either TfR (A, B) or LAMP-1 (B, C). Lysosomes in the cells in E and F were preloaded with dextran 647 as outlined in *Materials and Methods*. Arrowheads indicate phagosomes positive for TfR (A), LAMP-1 (C), or dextran (E). Arrows indicate phagosomes negative for TfR (A), LAMP-1 (B), or dextran (E). Scale bars, 5 μm. (B, D, F) Percentage of phagosomes positive for TfR, LAMP-1, or dextran at the indicated times. Data are means ± SEM from three independent experiments using cells from different donors. *$p < 0.05$; ***$p \leq 0.001$.

Additional determinants of the differential pH of M1 and M2 phagosomes

The luminal contents of phagosomes can associate with protons and influence the rate at which phagosomes acidify. We therefore compared the buffering capacity in M1 and M2 phagosomes by pulsing them with a weak base (Roos and Boron, 1981). Macrophages were challenged with fluorescein isothiocyanate (FITC)–labeled SOZ and 15–20 min after phagosome sealing

were treated with CcA and DPI to prevent the confounding pH changes associated with proton pumping or consumption, respectively. The change in phagosomal pH induced by addition of a defined concentration of NH_4^+ was measured and used to determine the buffering capacity (Figure 5, B and C). When measured ~25 min after phagosome sealing, the buffering power was similar in M1 and M2 phagosomes (25 ± 11 vs. 34 ± 11 mM/pH; Figure 5C).
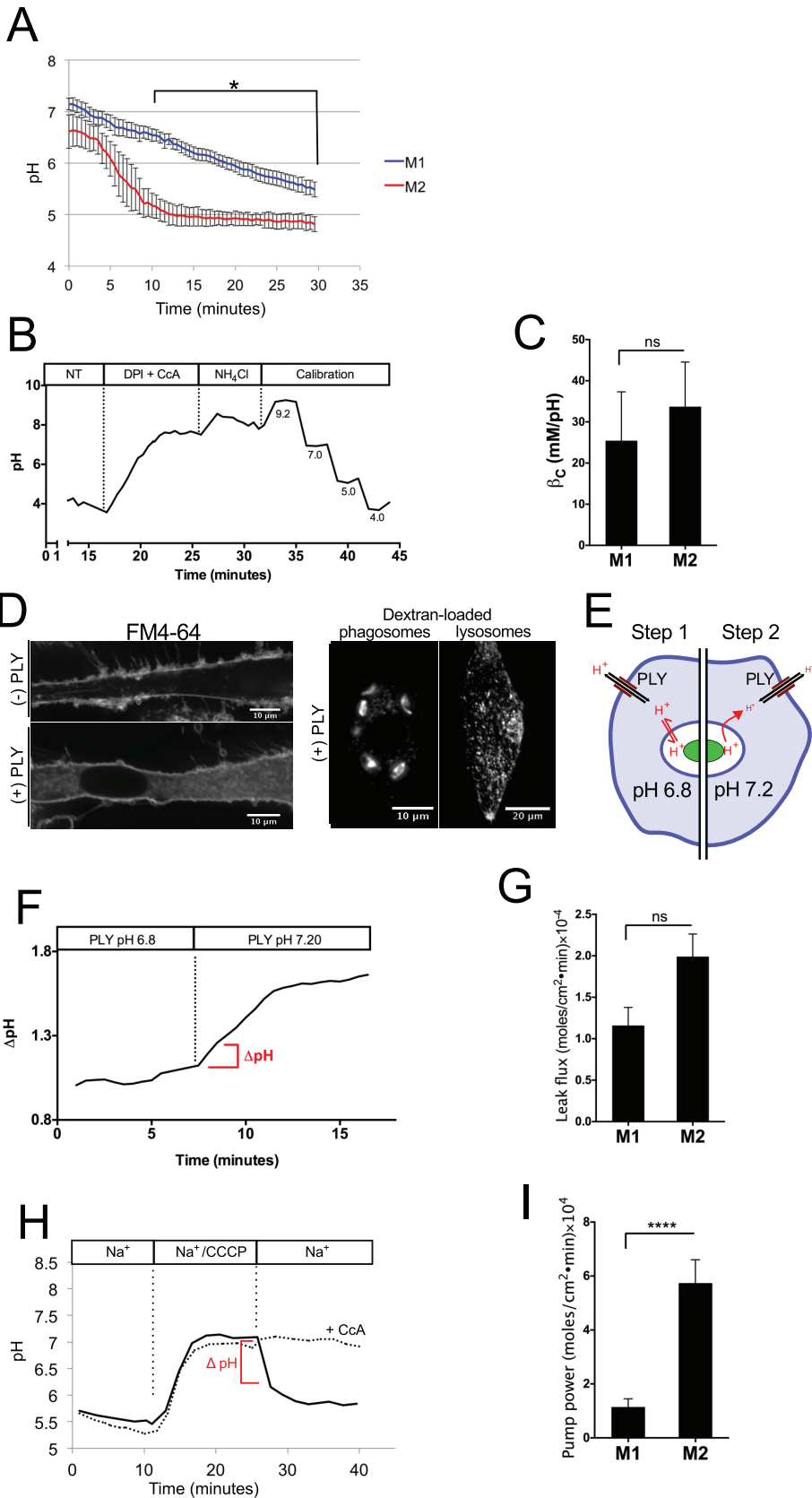
The rate and extent of acidification generated by the V-ATPases are also limited by the back-flux (leak) of protons. We therefore compared the passive proton (equivalent) permeability of phagosomes formed by M1 and M2 macrophages. This required the imposition of an identical proton-motive force across the membrane of both types of phagosomes. This was accomplished by inhibiting the V-ATPases as well as the oxidase—thereby maintaining the phagosomal pH near neutrality in both M1 and M2 cells—and

sealing, macrophages were treated with DPI and CcA, and the pH was monitored until a stable baseline was achieved. Then cells were pulsed with NH_4^+, and the change in pH was determined, followed by an in situ calibration as detailed in *Materials and Methods*. The graph shown is representative of multiple buffering capacity determinations in M1 and M2 macrophages. (C) Collated phagosomal buffering capacity (β_C) determinations obtained as in B. Data are means ± SEM from 11–15 independent determinations for each type. (D) Macrophages were labeled with FM4-64 before (left, top) or after (left, bottom) treatment with PLY. To determine whether PLY lysed internal membranes, cells were challenged with FITC-SOZ in the presence of fluid-phase dextran or pulsed for 1 h with dextran, which was then chased to lysosomes for 4 h, followed by treatment with PLY. Images were obtained by confocal microscopy. Scale bars, 10 µm. (E, G) M1 and M2 cells were challenged with FITC-SOZ, and 15–20 min after phagosome sealing, determination of H^+ leak flux was performed in two steps. In step 1, cells were treated with 2 µM CcA and permeabilized with PLY at pH 6.8, and the phagosome was allowed to equilibrate to pH 6.8. After acquisition of baseline readings at pH 6.8, the cells were transferred to buffer pH 7.2 with PLY (step2). The change in pH over time was recorded and used to determine the H^+ leak flux. The graph in F is representative of multiple similar experiments. (G) Collated determinations of H^+ leak flux. Data are means ± SEM of ≥11 independent determinations in M1 and M2 macrophages. (H) Phagosomal proton-pumping activity was determined by challenging macrophages with FITC-SOZ and allowing acidification to proceed in the presence of 10 µM DPI. Between 10 and 15 min after phagosome sealing, 1 µM CCCP was added. After the phagosomal pH equilibrated near neutral pH, CCCP was washed out with 2% fat-free BSA, and the ensuing pH change was recorded to determine pump activity. Where indicated, 2 µM CcA was added after BSA to assess the contribution of the V-ATPase. (H) A representative trace. (I) Means ± SEM from eight or nine independent determinations for each cell type. *$p < 0.05$, ***$p \leq 0.001$.

FIGURE 5: Determinants of phagosomal pH in M1 and M2 macrophages. (A) Macrophages were challenged with FITC-SOZ in the presence of 10 µM DPI, and phagosomal pH was determined every 30 s for the first 30 min of maturation, as described in *Materials and Methods*. The pH traces show the mean ± SEM of 4–16 independent determinations. (B) M1 and M2 macrophages were challenged with FITC-SOZ. Between 15 and 20 min after phagosome
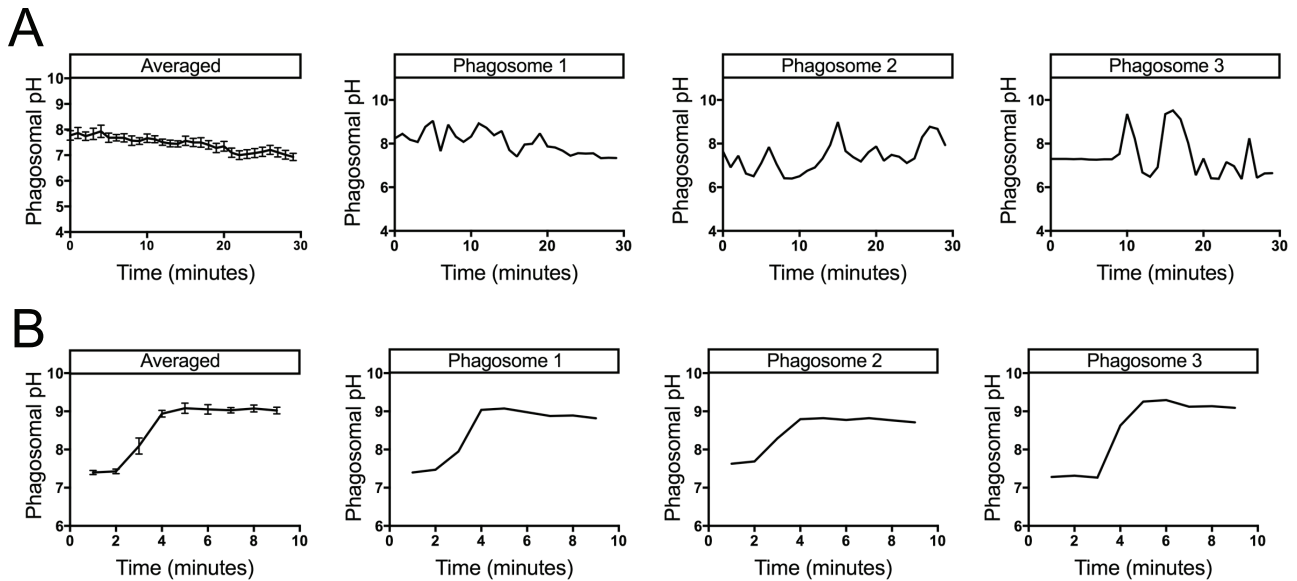
FIGURE 6: Phagosomal pH oscillations in M1 macrophages. (A) M1 macrophages were challenged with SNARF1-SOZ, and, upon particle uptake, pH measurements were acquired every minute for 30 min. The leftmost trace represents the mean ± SEM of 16 determinations. Three individual experiments are shown to the right of the averaged trace, to highlight the characteristic pH oscillations. (B) M1 macrophages were challenged with SNARF1-SOZ in the presence of 100 μM Zn^{2+}. The leftmost trace represents the mean ± SEM of eight determinations. Three individual experiments are shown to the right of the averaged trace.

suddenly altering the cytosolic pH to generate a transmembrane [H+] gradient (Figure 5E). To gain access to the cytosol while maintaining the integrity of the phagosomal membrane, we treated the cells with pneumolysin (PLY), a *Streptococcus pneumoniae* toxin that, like other cholesterol-dependent cytolysins, selectively permeabilizes the plasma membrane (Alouf, 2000; Tilley *et al.*, 2005). The effectiveness of the permeabilization procedure was verified using the membrane-impermeant dye FM4-64 (molecular weight 789), which stained only the outer leaflet of the plasmalemma in intact cells but labeled endomembranes after treatment with PLY (Figure 5D). Under comparable conditions, dextran preloaded into either phagosomes or lysosomes remained trapped (Figure 5D), indicating that the limiting membrane of these organelles was not disrupted by PLY.

Figure 5F illustrates a typical measurement of phagosomal pH in cells that were challenged with FITC-labeled SOZ, treated with CcA and DPI ~15–20 min after phagosome sealing, and permeabilized with PLY. The phagosomal pH, which was stable near pH 6.8 when the cells were permeabilized in medium of pH 6.8, underwent a gradual alkalosis when a step change in the extracellular—and hence also the cytosolic—pH (to 7.2) was applied. Under these conditions, the initial rate of acidification provided a reliable measure of the passive (leak) permeability. The results of multiple such experiments, which are summarized in Figure 5G, revealed that the H+ (equivalent) leak flux, calculated taking the corresponding buffering power into consideration, was moderately smaller in M1 phagosomes (1.16 × 10^{-4} mole/cm^2 min) than in M2 phagosomes (1.99 × 10^{-4} mole/cm^2 min), although the difference was not statistically significant.

Finally, we compared the proton pumping activity of M1 and M2 phagosomes. As before, the cells were treated with DPI to eliminate proton consumption by the oxidase. To obviate the variability introduced by the progressive delivery of V-ATPases to phagosomes during maturation, we allowed the phagosomes to mature for 15–20 min before measuring their pumping rate. This was accomplished by dissipating the existing acidification using the protonophore carbonyl cyanide *m*-chlorophenyl hydrazone

(CCCP), which was then abruptly removed by washing the cells with defatted albumin (Figure 5H). Removal of CCCP unleashed an acidification that was obliterated by addition of CcA, confirming mediation by V-ATPases. The proton pumping activity was estimated from the initial rate of acidification, considering the appropriate buffering power, and the results are collated in Figure 5I. Average phagosomal pump activity was markedly lower in M1 than in M2 macrophages. Thus the major factor accounting for the reduced rate of acidification of M1 phagosomes is reduced proton-pumping activity.

M1 macrophages exhibit oscillations in phagosomal pH due to the intermittent opening of voltage-gated proton channels

Whereas the phagosomal pH in M1 macrophages was routinely more alkaline than that of M2 macrophages, it was not constant over time. The variability, which is discernible in the averaged results illustrated in Figure 1A (replicated for reference in Supplemental Figure S4A), becomes more manifest when individual experiments are displayed (Supplemental Figure S4A). Such pH oscillations were unique to M1 phagosomes, as they were never observed in M2 phagosomes (Supplemental Figure S5A). Because fluorescein is best suited for pH measurements near its pK_a (6.3), we confirmed the occurrence of oscillations near and above neutral pH using SOZ covalently labeled with SNARF1 ($pK_a = 7.5$), a fluorophore better suited for pH determinations in the alkaline range (Figure 6A).

We next addressed the source of this oscillatory behavior. NADPH oxidase activity was required for the pH fluctuations, which were eliminated by treatment with DPI (Supplemental Figure S5B). The oxidase, which is electrogenic, generates a membrane potential that curtails its own activity; this antagonistic potential can in turn be relieved by the activation of H_V1 voltage-gated proton channels, restoring the ability of the oxidase to generate superoxide (DeCoursey and Cherny, 1993; Kapus *et al.*, 1993; Schrenzel *et al.*, 1998; DeCoursey *et al.*, 2000). We speculated that the phagosomal pH oscillations

observed in M1 macrophages might be a consequence of robust, yet self-limiting NADPH oxidase activity, punctuated by intermittent opening of H_V1 channels. Two approaches were used to test this hypothesis. First, we added Zn^{2+} at the time of phagosome formation; this cation is a potent inhibitor of the proton channels (Henderson et al., 1988). As illustrated in Figure 6B and Supplemental Figure S4B, this resulted in a large, sustained alkalinization of the phagosomal lumen, consistent with monotonic activation of the oxidase without intervening activation of H_V1 channels. Second, we used cells treated with valinomycin. Conductive influx of cytosolic K^+, catalyzed by the ionophore, can in principle compensate the charge differential created by NADPH oxidase–mediated electron transfer. This would preclude the generation of the transmembrane voltage required to open H_V1 channels. In accordance with this prediction, the pH oscillations attributed to intermittent opening of H_V1 were absent in phagosomes treated with valinomycin (Supplemental Figure S4C). We therefore concluded that the observed pH fluctuations reflect cycles of proton consumption, by dismutation of superoxide, interspersed with bouts of electrically driven proton influx, a result of activation of H_V1.

DISCUSSION

Here we report striking differences in the pH changes that follow phagosome sealing in M1 versus M2 macrophages. In agreement with previous measurements in primary murine macrophages (Lukacs et al., 1991) and monocyte/macrophage cell lines (Hackam et al., 1997), we found that phagosomes formed by human M2 macrophages undergo a rapid, monotonic acidification to pH ≤5. In sharp contrast, phagosomes in M1 cells fail to acidify and instead display waves of alkalinization followed by a return to near neutrality. Impaired phagosomal acidification had been observed in neutrophils and dendritic cells (Segal et al., 1981; Jankowski et al., 2002; Savina et al., 2006, 2009; Jancic et al., 2007; Mantegazza et al., 2008), where it was attributed to proton consumption upon dismutation of superoxide generated by NOX2. This mechanism also contributes to the failure of human M1 phagosomes to acidify and partially accounts for the differences between M1 and M2 cells. The latter were shown to express considerably lower amounts of the membrane-associated subunits of NOX2, which reside only transiently in the phagosomal membrane and, as a consequence, generate markedly lower amounts of superoxide. It is noteworthy, however, that polarized murine macrophages behave in a different manner; phagosomes formed by M1 macrophages become acidic (Yates et al., 2007; Balce et al., 2011), an observation we were able to replicate (unpublished data). In this regard, it is interesting that polarization toward the M1 phenotype induces expression of nitric oxide synthase in murine but not in human macrophages (Mantovani et al., 2004; Schneemann and Schoeden, 2007). Nitric oxide can react with superoxide (Wink and Mitchell, 1998; Wink et al., 1999, 2011), limiting its availability and therefore its ability to consume luminal H^+. It is also conceivable that murine M1 cells produce comparatively lower amounts of superoxide, relying instead on nitric oxide for microbial killing.

In accordance with the preceding discussion, inhibition of the oxidase eliminated the alkaline pH oscillations observed in untreated human M1 phagosomes, yielding instead a gradual acidification. However, even in the absence of NOX2 activity, significant differences in the rate of acidification persisted between M1 and M2 cells (Figure 5). Clearly, factors other than the unequal oxidase activity contribute to their differential pH regulation. A systematic analysis of the principal determinants of acidification revealed that, in addition to the elevated NOX2 activity, M1 phagosomes have a similar buffering power and passive permeability to H^+ equivalents but significantly lower rates of proton pumping (Figure 5), resulting in a reduced rate of acidification.

The lower proton pumping activity of M1 phagosomes suggests that fusion with V-ATPase–bearing organelles was less effective than in M2 phagosomes, a notion validated by the experiments of Figure 4. Was this the cause or a consequence of the reduced acidification? Dissipation of the luminal pH was found earlier to prolong the interaction of phagosomes with early endosomes and impair their fusion with lysosomes (Gordon et al., 1980; Hart and Young, 1991). It was therefore conceivable that other factors that modify the luminal pH might in turn affect the kinetics of phagosome maturation. To address this possibility, we analyzed the rate of acquisition of late endosomal/lysosomal markers by phagosomes while manipulating their luminal pH. As illustrated in Supplemental Figure S6, addition of NH_4^+ and CcA to counteract the acidification of M2 phagosomes reduced their rate of LAMP1 acquisition yet had no significant effect on M1 phagosomes, which are intrinsically unable to acidify. Conversely, inhibition of the NADPH oxidase, which promotes acidification in M1 phagosomes, accelerated LAMP1 acquisition by M1 but not by M2 phagosomes. Thus it appears that H^+ consumption by superoxide contributes to the delayed maturation and hence the reduced recruitment of V-ATPases to phagosomes in M1 cells.

Unexpectedly, we found that acidification was not entirely prevented in M1 phagosomes after treatment with concentrations of CcA expected to fully inhibit V-ATPase activity (Supplemental Figure S7A). Indeed, comparable concentrations completely eliminated the acidification of M2 phagosomes (Figure 1B). We therefore investigated this noncanonical, V-ATPase–independent mechanism of luminal acidification. Net influx of cytosolic H^+ (equivalents) was found to account for this effect. As shown in Supplemental Figure S7B, in cells treated with both DPI and CcA, the cytosol undergoes significant acidification during the course of phagocytosis, likely reflecting metabolic acid generation and/or net H^+ leakage from acidic organelles into the cytosol. Passive diffusion of cytosolic acid across the phagosomal membrane can therefore account for the V-ATPase-independent luminal acidification, which is of similar magnitude.

Unlike most previous studies, we performed continuous pH measurements in individual phagosomes. This modality enabled us to detect unprecedented oscillations of pH in M1 cells. The upstroke of the oscillations was eliminated by DPI and therefore attributed to H^+ consumption by dismutation of superoxide. These alkalinizing phases were interspersed with periods during which the pH returned toward neutrality. The latter were seemingly caused by intermittent opening of voltage-gated proton channels, likely H_V1. This was concluded based on 1) the elimination of the oscillations upon treatment with valinomycin, which provides a pathway for counterion transport that prevents the build-up of the transmembrane potential normally generated by the electrogenic activity of the oxidase, and 2) the inhibitory effects of Zn^{2+}, a potent blocker of Hv1 (Henderson et al., 1988; Morgan et al., 2009). We envisage the generation of superoxide to decelerate gradually as the electrical potential (negative inside) increases progressively, to the point where the threshold for Hv1 activation is reached. At this point, a sudden large influx of H^+ would not only collapse the transmembrane potential, but it would also provide needed substrate for the dismutation reaction and, of importance, would transiently reduce the luminal pH. The closure of the channels as the voltage collapses would reinitiate the alkalinization and electrical polarization cycle.

The sustained ROS production, near-neutral pH, and delayed maturation of M1 phagosomes have important functional consequences. It is generally accepted that, in dendritic cells, phagosomal

ROS production promotes antigen cross-presentation by negatively regulating proteolysis. Although there is debate as to whether it is the elevated pH or oxidative inactivation that reduces the activity of the proteolytic enzymes involved in antigen processing (Savina *et al.*, 2006; Mantegazza *et al.*, 2008; Rybicka *et al.*, 2010, 2012), it is clear that ROS production would similarly affect cross-presentation in M1 macrophages. Accordingly, enhanced antigen presentation is a hallmark of M1 macrophages (Lawrence and Natoli, 2011). On the other hand, the acidic lumen of phagosomes is considered essential for the effective clearance of engulfed material. In the case of apoptotic bodies and other debris ingested by M2 cells, digestion can proceed almost immediately, as their phagosomes rapidly acquire V-ATPases. In the case of pathogens ingested by M1 cells, their clearance must be preceded by microbial killing, which in many instances requires optimal and sustained generation of superoxide. Indeed, many intracellular pathogens known to thrive in the acidic phagolysosome, such as *Leishmania* spp., are particularly sensitive to ROS-mediated killing (Novais *et al.*, 2009, 2014). Thus delaying acidification for the sake of effective killing seems a reasonable price for M1 cells to pay.

In summary, the changes in luminal pH that ensue after phagosomal sealing are distinctly different in M1 and M2 human macrophages. M1 cells undergo an oscillatory alkalinization that reflects the alternating activity of NOX2 and Hv1, aimed at optimizing pathogen killing and maximizing antigen presentation at the expense of delayed degradation and elimination of microbial components. In M2 cells, by contrast, the oxidase and channel have little effect on the development of phagosomal acidification, which occurs rapidly for efficient hydrolysis and recycling of apoptotic cell components.

MATERIALS AND METHODS
Reagents
FITC, tetramethylrhodamine isothiocyanate, SNARF-1 succinimidyl ester, Zymosan A (*S. cerevisiae*) Bioparticles, diphenyl iodonium, FM4-64, SNARF-5f acetoxymethyl ester, dextran Alexa Fluor 647 (10,000 molecular weight), streptavidin Alexa Fluor 647, and nigericin were purchased from Life Technologies (Carlsbad, CA). NHS-biotin was purchased from Thermo-Scientific (Waltham, MA). Concanamycin A, nitroblue tetrazolium, luminol, catalase, superoxide dismutase, CCCP, valinomycin, and LPS were from Sigma-Aldrich (St. Louis, MO). GM-CSF, M-CSF, and IL-4 were purchased from R&D Systems (Minneapolis, MN). Pneumolysin was provided by A. Ratner (Columbia University, New York, NY). The mouse monoclonal antibodies 449 and 48 for p22 and gp91, respectively, were generously provided by A. Verhoeven and D. Roos (Central Laboratory of the Netherlands Blood Transfusion Service, Amsterdam, Netherlands) and A. Jesaitis and M. Quinn (Montana State University, Bozeman, MT). The mouse anti-human LAMP-1 antibody (Clone H4A3) was purchased from the Iowa Developmental Studies Hybridoma Bank (Iowa City, IA). The rabbit anti-human transferrin receptor antibody was purchased from Cell Signaling Technology (Beverley, MA). The APC-conjugated anti-human CD80 antibody, APC-conjugated anti-human CD1a, APC-conjugated mouse immunoglobulin (Ig) G1 κ isotype control, PE-conjugated mouse IgG1 κ isotype control, and PE-conjugated anti-human CD200r antibody were purchased from BioLegend (San Diego, CA). IRDye secondary goat anti-mouse antibodies were purchased from LI-COR (Lincoln, NE). All fluorophore-conjugated secondary antibodies used for immunofluorescence were from Jackson ImmunoResearch (West Grove, PA).

Solutions
The Na^+-rich medium contained 140 mM NaCl, 3 mM KCl, 1 mM $MgCl_2$, 1 mM $CaCl_2$, 5 mM glucose, and 20 mM 4-(2-hydroxyethyl)-1-piperazineethanesulfonic acid (HEPES) adjusted to pH 7.2 at 37°C. The K^+-rich medium contained 143 mM KCl, 1 mM $MgCl_2$, 1 mM $CaCl_2$, 5 mM glucose, and 20 mM HEPES or acetic acid, depending on the pH used for calibration. The osmolarity of all solutions was adjusted to between 285 and 295 mOsm. The cytosolic buffer contained 10 mM NaCl, 20 mM HEPES, 50 mM KCl, 2 mM K_2HPO_4, 90 mM potassium glutamate, 4 mM $MgCl_2$, 4 mM ethylene glycol tetraacetic acid, 2 mM $CaCl_2$, 4 mM ATP, 3 mM sodium pyruvate, and 15 µg/ml purified recombinant PLY; the final solution was adjusted to the pH indicated.

Macrophage and dendritic cell isolation and culture
Human peripheral blood mononuclear cells (PBMCs) were isolated from the blood of healthy donors by density gradient separation using Lympholyte-H (Cedarlane, Burlington, Canada). Monocytes were purified by adherence to glass coverslips in 12-well plates (3.0×10^6 PBMCs/well) and cultured for 5 d in RPMI 1640 supplemented with 10% fetal bovine serum, antibiotic/antimycotic (Multicell, Wisent, St-Bruno, Canada), and either 25 ng/ml GM-CSF (for M1 macrophages) or 25 ng/ml M-CSF (for M2 macrophages). After 5 d, macrophages were treated for an additional 2 d with either LPS (500 ng/ml) plus IFN-γ (10 ng/ml) or IL-4 (15 ng/ml) for M1 and M2 macrophages, respectively. For generation of monocyte-derived dendritic cells, monocytes were incubated with 25 ng/ml GM-CSF and 15 ng/ml IL-4 for 7 d.

Preparation of serum-opsonized zymosan
Dried Zymosan A Bioparticles were resuspended in phosphate-buffered saline (PBS) and sonicated to break up large aggregates. Zymosan was resuspended in 0.1 M sodium carbonate (pH 9.0 for isothiocyanates and 8.3 for succinimidyl esters). Reactive fluorophores (fluorescein isothiocyanate, SNARF-1 succinimidyl ester, or tetramethylrhodamine isothiocyanate) were dissolved in 0.1 M sodium carbonate at 1 mg/ml. The reaction was initiated by adding 0.1 mg of the probe to 1 mg of zymosan. The mixture was allowed to react for 1 h at 37°C with constant agitation. Unbound probe was removed by washing six times with PBS (pH 7.4), and labeled zymosan was stored at –20°C. Before phagocytosis assays, fluorophore-conjugated zymosan was resuspended in autologous human serum at 2 mg/ml and incubated at 37°C for 30 min with constant agitation. Zymosan was subsequently washed gently three times with PBS (pH 7.4) and used immediately.

pH measurements
Macrophages plated onto 18-mm coverslips were placed in a Chamlide magnetic coverslip holder, mounted onto a temperature-controlled stage (set to 37°C), and overlaid with HEPES-buffered RPMI. The macrophages were visualized with a Leica DM IRB microscope (Leica, Wetzlar, Germany). Serum-opsonized FITC or SNARF1-labeled zymosan was then added, and the cells were monitored for binding of zymosan. Once a cell was found that had bound fluorophore-labeled zymosan, pH measurements were performed by fluorescence ratiometric imaging using a filter wheel (Sutter Instruments, Novato, CA) to rapidly alternate between excitation filters. The fluorophore-labeled-zymosan was excited by light from an EXFO X-cite 120 lamp (ExFo Life Sciences, Quebec, Canada) transmitted through the appropriate excitation filters and directed to the sample using a dichroic mirror. The emitted light was captured by a charge-coupled device (CCD) camera (Cascade II; Photometrics, Tucson, AZ) after passing through an emission filter. MetaFluor (MDS Analytical Technologies, Sunnyvale, CA) software was used to control the filter wheel and camera.

An in situ calibration was performed for each phagosome after measurement. Samples were bathed in K^+-rich buffers ranging from

pH 4.5 to 9.6 containing 10 µg/ml nigericin. Images were taken 5 min after the addition of each calibration solution to ensure equilibration to the desired pH. The resulting fluorescence intensity ratio was plotted as a function of pH and fitted to a Boltzmann sigmoid that was used to interpolate ratios measured during phagosome maturation.

Buffering capacity, H+ leak flux, and proton pump activity determinations

The phagosomal buffering capacity was determined by measuring the change in pH induced by a pulse of the weak base NH_4^+ and calculated as described by Roos and Boron (1981). To estimate the phagosomal buffering capacity of M1 and M2 macrophages at equivalent pH, phagosomes were treated with 10 µM DPI and 2 µM CcA 15–20 min after phagosome sealing. At the desired pH, NH_4^+ was added to the bathing medium, and the resulting change in pH was recorded. Buffering power was measured between pH 6.3 and 7.4.

To eliminate variability due to different starting phagosomal pH values in M1 and M2 macrophages during measurements of H+ leak, the luminal pH and cytosolic pH were preestablished. To this end, ~15–20 min after phagosome sealing, cells were bathed in the cytosolic buffer described at pH 6.8 in the presence of DPI and CcA and the plasmalemma permeabilized with PLY. After the cytosol and luminal pH of the phagosome was allowed to equilibrate to pH 6.8, the bathing solution was switched to cytosolic buffer at pH 7.2. The resulting change in phagosomal pH was then recorded and used to estimate proton leakage. The passive (leak) H+ flux was calculated as the product of the initial rate of pH change times the buffering capacity, assuming an average phagosomal diameter of 4 µm (zymosan diameter ranges from 3 to 5 µm).

To calculate proton pump activity, the cells were treated with DPI, and phagosomes were left to acidify to between pH 5.5 and 6.0 in Na+-rich medium. Phagosomal pH was then dissipated by adding 1 µM CCCP. On equilibration, CCCP was washed out with 2% fat-free bovine serum albumin (BSA), and fresh Na+-rich medium was added either with or without CcA. Pump activity was calculated by multiplying the initial rate of change of pH by the buffering capacity, assuming a diameter of 4 µm to calculate the area of the phagosomal membrane.

Cytosolic pH measurements

Macrophages were incubated with the acetoxymethyl ester of SNARF-5f (20 µM) for 30 min at 37°C in Na+-rich medium. SOZ was then added to the cells, a cell engulfing particles was located, and cytosolic pH was determined by fluorescence ratiometric imaging using single excitation (540 nm) and dual emission (580 and 640 nm). An in situ calibration was performed for each cell as described. The control of the filter wheels, image acquisition, and analysis were performed using MetaFluor software.

Nitroblue tetrazolium assay

We added 10 µl of SOZ from a 2 mg/mL stock and NBT at the indicated concentration to cells growing on 18-mm coverslips. The coverslips placed in a 12-well plate were centrifuged to rapidly bring the SOZ in contact with the cells. Excess particles were removed by three washes with PBS. Cells were immediately visualized on a Leica DM IRB microscope, and images were taken every 30 s for 30 min.

Luminol assay

For luminol measurements, macrophages were plated and cultured in white-sided tissue culture plates (Corning Incorporated, Corning, NY). Just before the assay, macrophages were bathed in PBS containing 10 mM glucose (PBS-G) and 8 U/ml horseradish peroxidase

(HRP). SOZ was added to the macrophages, followed by centrifugation for 1 min. Excess SOZ was washed away with PBS-G. After washing, PBS-G containing 8 U/ml HRP and 50 µM luminol was added to the macrophages, and the plates were placed in a SpectraMax L luminometer (Molecular Devices, Sunnyvale, CA). Luminescence was measured every 2 min for a total of 10 min. Then SOD (50 U/ml) and catalase (2000 U/ml) were added to each well to eliminate extracellular ROS, and luminescence was recorded for an additional 80 min.

Confocal microscopy

Macrophages were challenged with 10 µl of fluorescent SOZ from a 2 mg/ml stock and centrifuged for 1 min. Excess SOZ was removed by three washes with PBS. Cells were incubated for an additional 4 min at 37°C, and then external SOZ was labeled with either fluorophore-labeled anti-human IgG or fluorophore-labeled streptavidin for 10 min on ice. Cells were washed three times with PBS and placed back at 37°C for the indicated time. Where indicated, cells were preloaded with fluorescent dextran with a 1-h pulse of dextran at 5 mg/ml, followed by a 3-h chase. At indicated time points, cells were fixed with either 2% paraformaldehyde or ice-cold methanol and immunostained with the indicated antibodies. Cells were imaged by spinning disk confocal microscopy on an Axiovert 200M with a 63× objective and an additional 1.5× magnifying lens (Carl Zeiss, Oberkochen, Germany). The microscope is equipped with diode-pumped solid-state lasers (440, 491, 561, 638, and 655 nm; Spectral Applied Research, Richmond Hill, ON, Canada) and a piezo focus drive. Images were acquired on a CCD camera (Hamamatsu Photonics, Hamamatsu, Japan) driven by Volocity software.

Flow cytometry

Macrophages were gently lifted from tissue-culture plates by incubation with cold PBS (Ca2+-, Mg2+-free) with 10 mM EDTA at pH 7.4 at 10°C. Cells were then resuspended in PBS/2% BSA at a concentration of 10^6 cells per 100 µl and labeled with fluorophore-conjugated primary antibodies at the dilution specified by the company from which the antibodies were purchased. Cells were incubated for 1 h on ice, followed by five washes with cold PBS/2% BSA and fixation with 2% PFA. Cells were passed through a cell strainer, run through an LSRII flow cytometer (BD Biosciences, Franklin Lakes, NJ), and analyzed using FlowJo software (Tree Star, Ashland, OR).

Immunoblotting

For immunoblot analysis, cells were washed three times with cold PBS and lysed using cold RIPA buffer. Fifty micrograms of protein was loaded and separated by 12% SDS–PAGE, transferred to a polyvinylidene fluoride membrane, and blocked in TBS 0.05%, Tween 20, and 5% nonfat milk for 1 h. Primary and secondary antibodies were added to the membrane in 2% fat-free milk. After washing with Tris-buffered saline/0.05% Tween-20, membranes were visualized on the Odyssey Fc (LI-COR, Lincoln,NE). Band intensity was quantified using ImageJ software.

Statistics

For statistical analysis, unpaired *t* tests were used with a 95% confidence interval. All data presented in the text and graphs are means and SE of at least three independent experiments.

REFERENCES

Alouf JE (2000). Cholesterol-binding cytolytic protein toxins. Int J Med Microbiol 290, 351–356.

Amezaga MA, Bazzoni F, Sorio C, Rossi F, Cassatella MA (1992). Evidence for the involvement of distinct signal transduction pathways in the regulation of constitutive and interferon gamma-dependent gene expression of NADPH oxidase components (gp91-phox, p47-phox, and p22-phox) and high-affinity receptor for IgG (Fc gamma R-I) in human polymorpho-nuclear leukocytes. Blood 79, 735–744.

Balce DR, Li B, Allan ER, Rybicka JM, Krohn RM, Yates RM (2011). Alternative activation of macrophages by IL-4 enhances the proteolytic capacity of their phagosomes through synergistic mechanisms. Blood 118, 4199–4208.

Blum JS, Wearsch PA, Cresswell P (2013). Pathways of antigen processing. Annu Rev Immunol 31, 443–473.

Casbon AJ, Long ME, Dunn KW, Allen LA, Dinauer MC (2012). Effects of IFN-γ on intracellular trafficking and activity of macrophage NADPH oxidase flavocytochrome b558. J Leukoc Biol 92, 869–882.

Cassatella MA, Bazzoni F, Flynn RM, Dusi S, Trinchieri G, Rossi F (1990). Molecular basis of interferon-gamma and lipopolysaccharide enhancement of phagocyte respiratory burst capability. Studies on the gene expression of several NADPH oxidase components. J Biol Chem 265, 20241–20246.

Dahlgren C, Karlsson A, Bylund J (2007). Measurement of respiratory burst products generated by professional phagocytes. Methods Mol Biol 412, 349–363.

DeCoursey TE, Cherny VV (1993). Potential, pH, and arachidonate gate hydrogen ion currents in human neutrophils. Biophys J 65, 1590–1598.

DeCoursey TE, Cherny VV, Zhou W, Thomas LL (2000). Simultaneous activation of NADPH oxidase-related proton and electron currents in human neutrophils. Proc Natl Acad Sci USA 97, 6885–6889.

Galli SJ, Borregaard N, Wynn TA (2011). Phenotypic and functional plasticity of cells of innate immunity: macrophages, mast cells and neutrophils. Nat Immunol 12, 1035–1044.

Gordon AH, Hart PD, Young MR (1980). Ammonia inhibits phagosome-lysosome fusion in macrophages. Nature 286, 79–80.

Hackam DJ, Rotstein OD, Zhang WJ, Demaurex N, Woodside M, Tsai O, Grinstein S (1997). Regulation of phagosomal acidification. Differential targeting of Na+/H +exchangers, Na+/K+-ATPases, and vacuolar-type H+-ATPases. J Biol Chem 272, 29810–29820.

Hart PD, Young MR (1991). Ammonium chloride, an inhibitor of phagosome-lysosome fusion in macrophages, concurrently induces phagosome-endosome fusion, and opens a novel pathway: studies of a pathogenic mycobacterium and a nonpathogenic yeast. J Exp Med 174, 881–889.

Henderson LM, Chappell JB, Jones OT (1988). Superoxide generation by the electrogenic NADPH oxidase of human neutrophils is limited by the movement of a compensating charge. Biochem J 255, 285–290.

Hufford MM, Kim TS, Sun J, Braciale TJ (2011). Antiviral CD8+ T cell effector activities in situ are regulated by target cell type. J Exp Med 208, 167–180.

Jaguin M, Houlbert N, Fardel O, Lecureur V (2013). Polarization profiles of human M-CSF-generated macrophages and comparison of M1-markers in classically activated macrophages from GM-CSF and M-CSF origin. Cell Immunol 281, 51–61.

Jancic C, Savina A, Wasmeier C, Tolmachova T, El-Benna J, Dang PM, Pascolo S, Gougerot-Pocidalo MA, Raposo G, Seabra MC, et al. (2007). Rab27a regulates phagosomal pH and NADPH oxidase recruitment to dendritic cell phagosomes. Nat Cell Biol 9, 367–378.

Jankowski A, Scott CC, Grinstein S (2002). Determinants of the phagosomal pH in neutrophils. J Biol Chem 277, 6059–6066.

Kapus A, Romanek R, Qu AY, Rotstein OD, Grinstein S (1993). A pH-sensitive and voltage-dependent proton conductance in the plasma membrane of macrophages. J Gen Physiol 102, 729–760.

Lawrence T, Natoli G (2011). Transcriptional regulation of macrophage polarization: enabling diversity with identity. Nat Rev Immunol 11, 750–761.

Lukacs GL, Rotstein OD, Grinstein S (1991). Determinants of the phagosomal pH in macrophages. In situ assessment of vacuolar H(+)-ATPase activity, counterion conductance, and H+ "leak". J Biol Chem 266, 24540–24548.

Mantegazza AR, Savina A, Vermeulen M, Pérez L, Geffner J, Hermine O, Rosenzweig SD, Faure F, Amigorena S (2008). NADPH oxidase controls phagosomal pH and antigen cross-presentation in human dendritic cells. Blood 112, 4712–4722.

Mantovani A, Sica A, Sozzani S, Allavena P, Vecchi A, Locati M (2004). The chemokine system in diverse forms of macrophage activation and polarization. Trends Immunol 25, 677–686.

McWhorter FY, Wang T, Nguyen P, Chung T, Liu WF (2013). Modulation of macrophage phenotype by cell shape. Proc Natl Acad Sci USA 110, 17253–17258.

Morgan D, Capasso M, Musset B, Cherny VV, Ríos E, Dyer MJ, DeCoursey TE (2009). Voltage-gated proton channels maintain pH in human neutrophils during phagocytosis. Proc Natl Acad Sci USA 106, 18022–18027.

Mosser DM, Edwards JP (2008). Exploring the full spectrum of macrophage activation. Nat Rev Immunol 8, 958–969.

Novais FO, Nguyen BT, Beiting DP, Carvalho LP, Glennie ND, Passos S, Carvalho EM, Scott P (2014). Human classical monocytes control the intracellular stage of Leishmania braziliensis by reactive oxygen species. J Infect Dis 209, 1288–1296.

Novais FO, Santiago RC, Báfica A, Khouri R, Afonso L, Borges VM, Brodskyn C, Barral-Netto M, Barral A, de Oliveira CI (2009). Neutrophils and macrophages cooperate in host resistance against Leishmania braziliensis infection. J Immunol 183, 8088–8098.

Roos A, Boron WF (1981). Intracellular pH. Physiol Rev 61, 296–434.

Rybicka JM, Balce DR, Chaudhuri S, Allan ER, Yates RM (2012). Phagosomal proteolysis in dendritic cells is modulated by NADPH oxidase in a pH-independent manner. EMBO J 31, 932–944.

Rybicka JM, Balce DR, Khan MF, Krohn RM, Yates RM (2010). NADPH oxidase activity controls phagosomal proteolysis in macrophages through modulation of the lumenal redox environment of phagosomes. Proc Natl Acad Sci USA 107, 10496–10501.

Savina A, Jancic C, Hugues S, Guermonprez P, Vargas P, Moura IC, Lennon-Duménil AM, Seabra MC, Raposo G, Amigorena S (2006). NOX2 controls phagosomal pH to regulate antigen processing during crosspresentation by dendritic cells. Cell 126, 205–218.

Savina A, Peres A, Cebrian I, Carmo N, Moita C, Hacohen N, Moita LF, Amigorena S (2009). The small GTPase Rac2 controls phagosomal alkalinization and antigen crosspresentation selectively in CD8(+) dendritic cells. Immunity 30, 544–555.

Schneemann M, Schoeden G (2007). Macrophage biology and immunology: man is not a mouse. J Leukoc Biol 81, 579; discussion, 580.

Schrenzel J, Serrander L, Bánfi B, Nüsse O, Fouyouzi R, Lew DP, Demaurex N, Krause KH (1998). Electron currents generated by the human phagocyte NADPH oxidase. Nature 392, 734–737.

Segal AW, Geisow M, Garcia R, Harper A, Miller R (1981). The respiratory burst of phagocytic cells is associated with a rise in vacuolar pH. Nature 290, 406–409.

Short KR, Grant EJ, Vissers M, Reading PC, Diavatopoulos DA, Kedzierska K (2013). A novel method linking antigen presentation by human monocyte-derived macrophages to CD8(+)T cell polyfunctionality.. Front Immunol 4, 389.

Sokolovska A, Becker CE, Ip WK, Rathinam VA, Brudner M, Paquette N, Tanne A, Vanaja SK, Moore KJ, Fitzgerald KA, et al. (2013). Activation of caspase-1 by the NLRP3 inflammasome regulates the NADPH oxidase NOX2 to control phagosome function. Nat Immunol 14, 543–553.

Steinberg BE, Grinstein S (2007). Assessment of phagosome formation and maturation by fluorescence microscopy. Methods Mol Biol 412, 289–300.

Tilley SJ, Orlova EV, Gilbert RJ, Andrew PW, Saibil HR (2005). Structural basis of pore formation by the bacterial toxin pneumolysin. Cell 121, 247–256.

Tsang AW, Oestergaard K, Myers JT, Swanson JA (2000). Altered membrane trafficking in activated bone marrow-derived macrophages. J Leukoc Biol 68, 487–494.

Uderhardt S, Herrmann M, Oskolkova OV, Aschermann S, Bicker W, Ipseiz N, Sarter K, Frey B, Rothe T, Voll R, et al. (2012). 12/15-lipoxygenase orchestrates the clearance of apoptotic cells and maintains immunologic tolerance. Immunity 36, 834–846.

Wink DA, Hines HB, Cheng RY, Switzer CH, Flores-Santana W, Vitek MP, Ridnour LA, Colton CA (2011). Nitric oxide and redox mechanisms in the immune response. J Leukoc Biol 89, 873–891.

Wink DA, Mitchell JB (1998). Chemical biology of nitric oxide: insights into regulatory, cytotoxic, and cytoprotective mechanisms of nitric oxide. Free Radic Biol Med 25, 434–456.

Wink DA, Vodovotz Y, Grisham MB, DeGraff W, Cook JC, Pacelli R, Krishna M, Mitchell JB (1999). Antioxidant effects of nitric oxide. Methods Enzymol 301, 413–424.

Yates RM, Hermetter A, Taylor GA, Russell DG (2007). Macrophage activation downregulates the degradative capacity of the phagosome. Traffic 8, 241–250.

Zizzo G, Hilliard BA, Monestier M, Cohen PL (2012). Efficient clearance of early apoptotic cells by human macrophages requires M2c polarization and MerTK induction. J Immunol 189, 3508–3520.